Leaf-inspired graphene/MnO networks encapsulating Co nanoparticles through micro-nano structural engineering for enhanced photo-stimulated rechargeable Zn-air battery

Peitao Liu,*[a] Zihan Zhang,[a] Chongyang Yang,[a] Junming Zhang[b] and Daqiang Gao*[c]

[a]*Key Laboratory of Materials Physics and Functional Devices of Baoji, Institute of Physics & Optoelectronics Technology, Baoji University of Arts and Sciences, Baoji 721016, P.R. China*;

Email: liupt@bjwlxy.edu.cn

[b]*State Key Laboratory of New Ceramics and Fine Processing, School of Materials Science and Engineering, Tsinghua University, Beijing 100084, China*;

[c]*Key Laboratory for Magnetism and Magnetic Materials of MOE, Key Laboratory of Special Function Materials and Structure Design of MOE, Lanzhou University, Lanzhou 730000, P. R. China*;

E-mail: gaodq@lzu.edu.cn

1. Experimental section

1.1. Material characterization

The crystal structures of the fabricated samples were characterized by X-ray powder diffraction (XRD; X'pert Pro Philips with Cu K radiation), while their morphologies and microstructures were examined by transmission electron microscopy (TEM; Tecnai G2 F30, FEI). Chemical states and bonding characteristics were analyzed via X-ray photoelectron spectroscopy (XPS; Kratos AXIS Ultra) and Raman spectroscopy (Jobin-Yvon LabRam HR80). N_2 adsorption/desorption curves were recorded at a desorption temperature of 250 °C using a Micrometrics ASAP 2020 V403 device to obtain specific surface areas and pore diameters. Bandgap values were determined by ultraviolet-visible (UV-vis) diffuse reflectance spectroscopy using Shimadzu's integrating sphere method.

1.2. Electrochemical characterization.

Both the OER and ORR electrochemical processes were performed at room temperature (25 ± 0.5 °C). All electrochemical tests were conducted on a CHI 760 electrochemical workstation (CHI Instruments, Shanghai Chenhua Instrument Co., Ltd., China) using a three-electrode system. A sample coated with carbon cloth or a rotating ring-disk electrode (RRDE) was used as the working electrode, saturated Ag/AgCl served as the reference electrode, and a Pt plate was utilized as the counter electrode. In this study, the measured potential (vs. Ag/AgCl) was converted into a potential versus a reversible hydrogen electrode (RHE), and iR correction was performed according to the Nernst equation ($E_{RHE} = E_{Ag/AgCl} + 0.197 + 0.059$ pH). For the ORR reaction, a catalytic ink was prepared by dissolving 3 mg of the catalyst in 1470 μL N,N-dimethylformamide (DMF) and 30 μL Nafion. The ink was dripped onto the rotating disk working electrode (RDE) at a load of 0.2 mg/cm^2 and dried at room temperature. All ORR properties were tested at a rotation speed of 1600 RPM and O_2 saturation in a 0.1 M KOH solution. For the OER, 10 mg of the catalyst was dissolved in 970 μL DMF and 30 μL Nafion. The obtained catalytic ink was dripped onto the working electrode at a load of 2 mg/cm^2 and dried at room temperature. OER parameters were determined in a 1 M KOH solution. All photoelectric reaction tests were performed using 175 W metal halide lamps to examine the photoelectric catalytic performance of the studied samples.

1.3. Zinc-air battery measurement

A polished zinc plate was used as the anode, a catalyst with a load of 2 mg /cm^2 was utilized as the air cathode, and a solution containing 6 M KOH and 0.2 M zinc acetate was employed as the electrolyte. Rechargeable ZABs were assembled using carbon fiber paper. To construct micro-solid ZABs, MnO/Co@N-C was used as the air cathode, a polished Zn plate was employed as the anode, and an alkaline hydrogel polymer served as the electrolyte. Battery performance was evaluated by a potentiostat (CHI 760E, Shanghai Chenhua Instrument Co., Ltd.) and Blue Power testing system. Under the same conditions, 20% Pt/C was used as the air cathode in ZABs. All photoelectric cells were irradiated by 175 W metal halide lamps to investigate their photoelectric performance.

1.4. Calculation details

The density functional theory (DFT) simulations of the catalysts were carried out by the Vienna ab initio simulation package (VASP). The standard generalized gradient approximation (GGA) parametrized by Perdew, Burke and Ernzerhof (PBE) was employed as the exchange-correlation potential. The energy cutoff of the plane waves used for expanding electronic wave functions is 400 eV. A Monkhorst–Pack k-point mesh of 4×4×4 was used for geometry optimization and electronic property calculations. Both atomic positions and cell parameters were optimized until the residual forces were below 0.01 eV/Å.

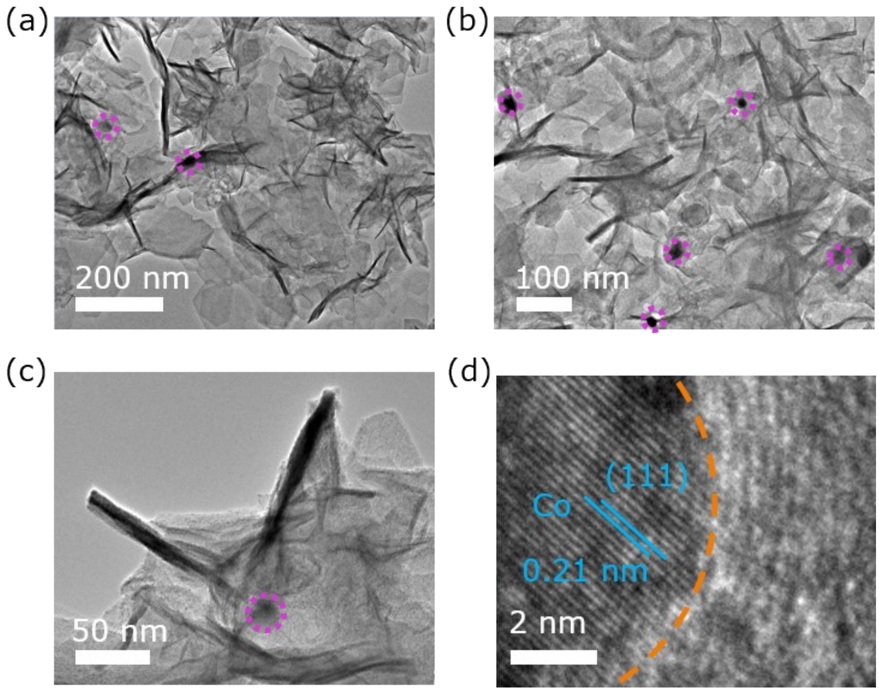

Fig. S1 (a)-(c) The TEM and (d) HRTEM images of MnO/Co@N-C catalyst.

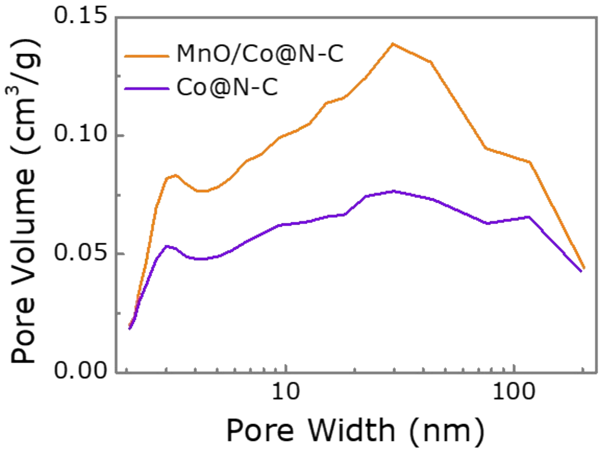

Fig. S2 The pore width of Co@N-C and MnO/Co@N-C catalyst.

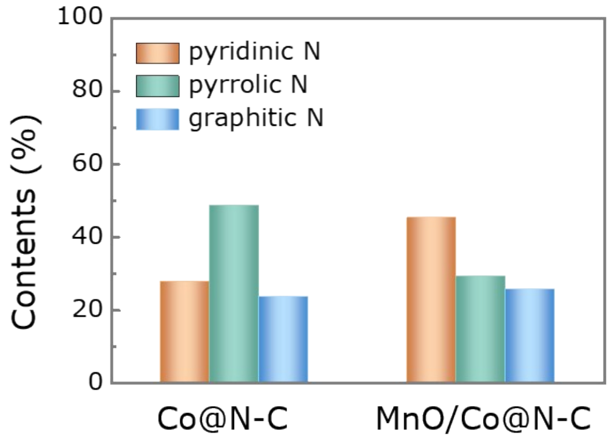

Fig. S3 The fitting peak area data of N 1s for MnO/Co@N-C and Co@N-C catalysts.

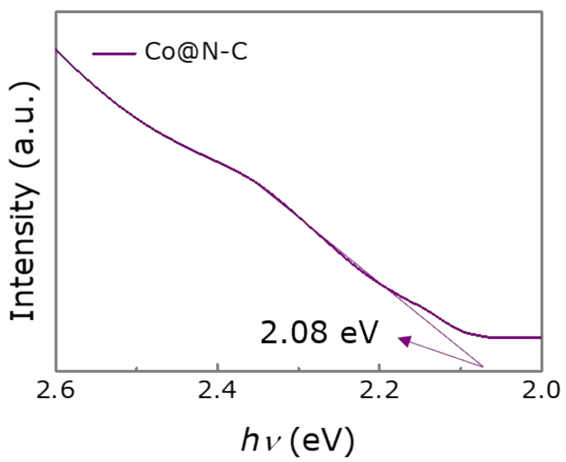

Fig. S4 The UV/Vis spectrum for Co@N-C catalyst.

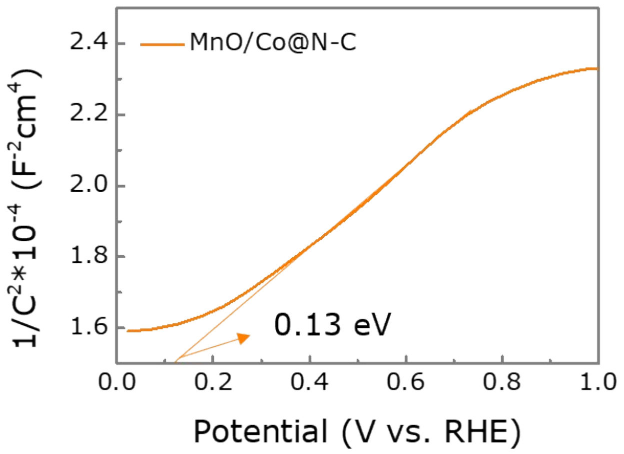

Fig. S5 Mott-Schotty plots of MnO/Co@N-C catalyst.

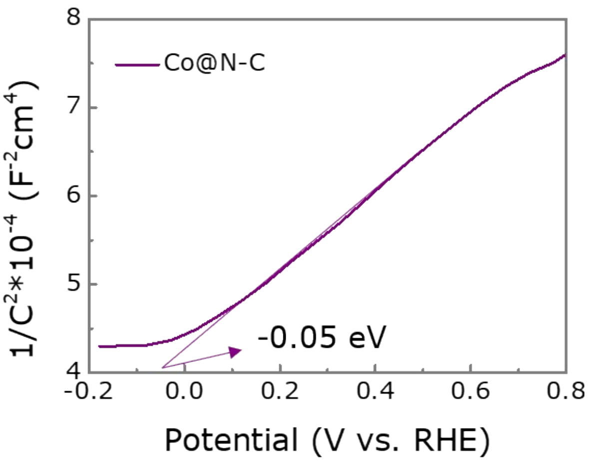

Fig. S6 Mott-Schotty plots of Co@N-C catalyst.

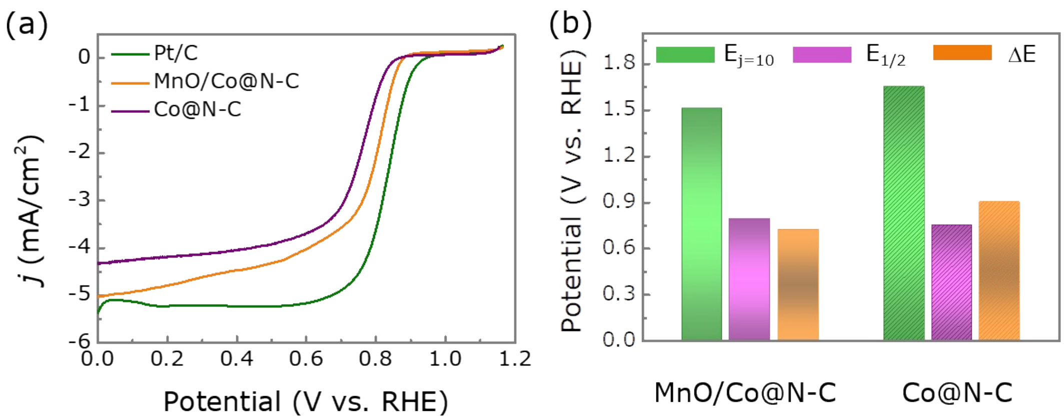

Fig. S7 (a) LSV curves of ORR for the MnO/Co@N-C, Co@N-C and Pt/C catalysts at 1600 rpm.

(b) The values of $E_{j=10}$, $E_{1/2}$ and the corresponding ΔE values ($\Delta E = E_{j=10} - E_{1/2}$).

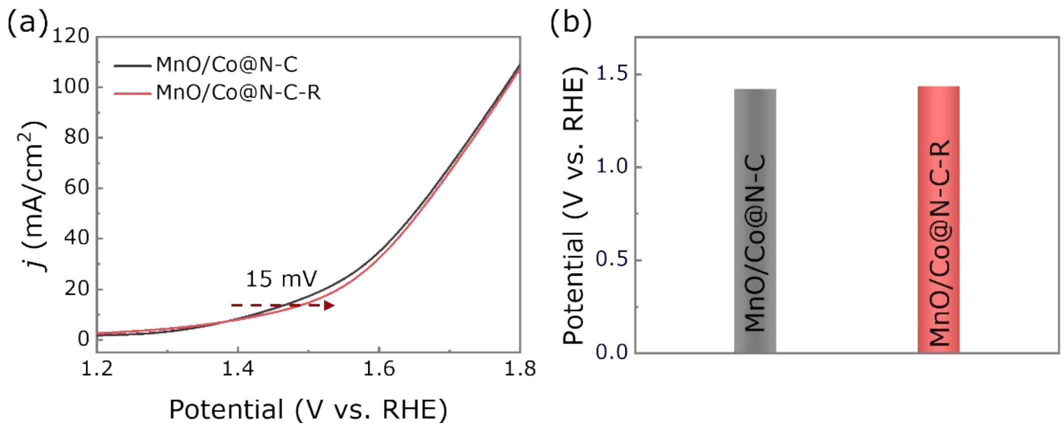

Fig. S8 (a) and (b) OER curves for the MnO/Co@N-C and MnO/Co@N-C-R catalysts under illumination conditions.

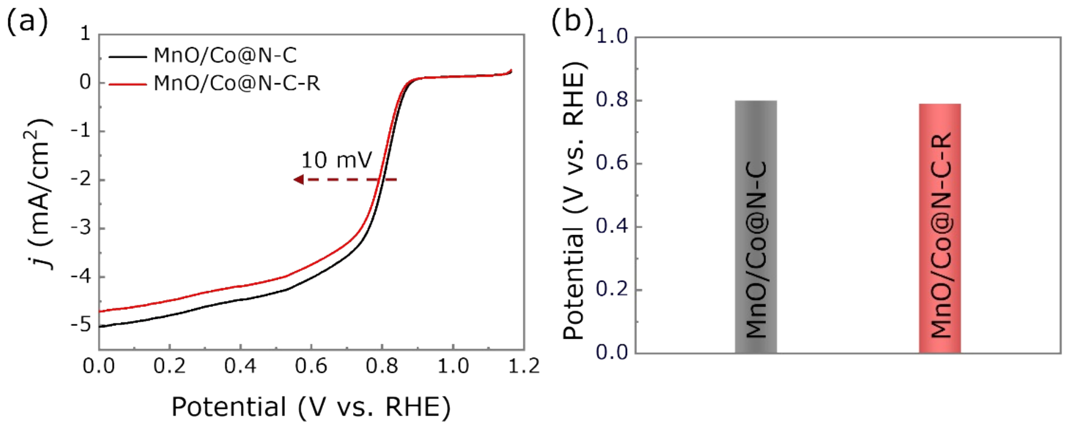

Fig. S9 (a) and (b) OER curves for the MnO/Co@N-C and MnO/Co@N-C-R catalysts under illumination conditions.

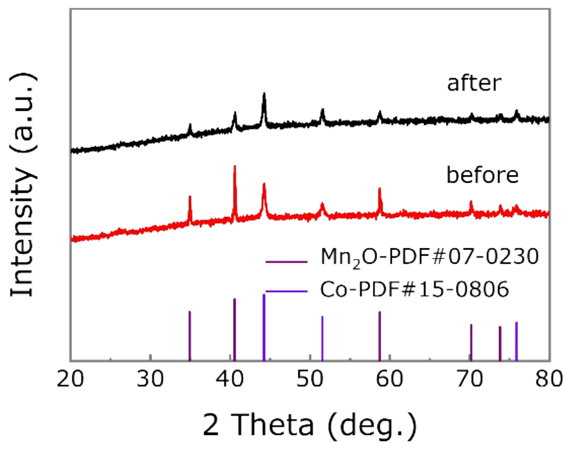

Fig. S10 The XRD results for the MnO/Co@N-C before and after charge-discharge cycles.

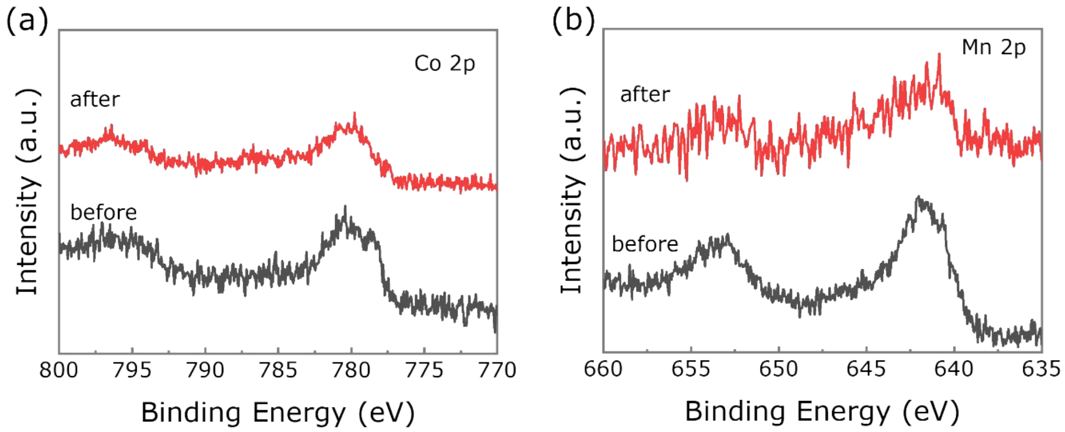

Fig. S11 (a) The Co 2p and (b) Mn 2p XPS spectrum of MnO/Co@N-C before and after charge-discharge cycles.

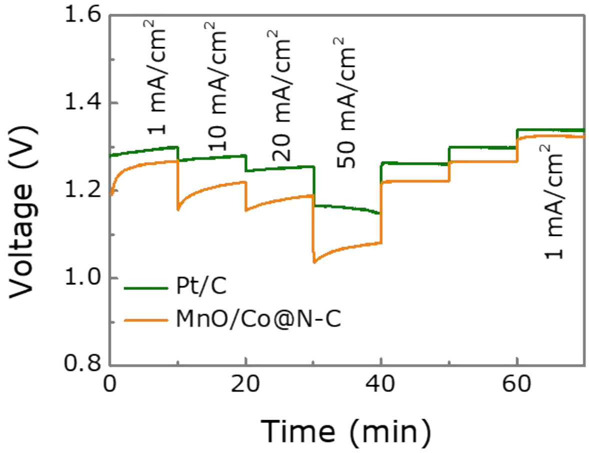

Fig. S12 Discharge curves of the MnO/Co@N-C and Pt/C based ZABs at different current densities, respectively.

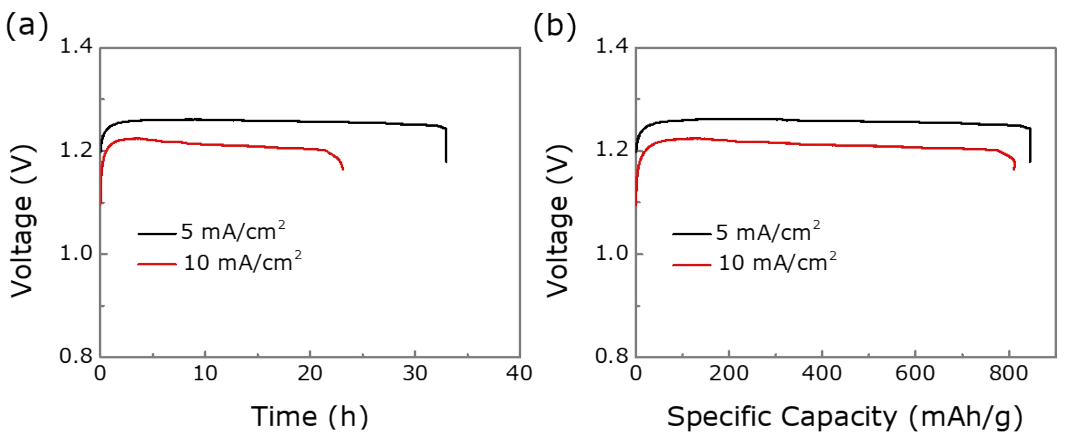

Fig. S13 (a) Discharge curves at the current density of 5 mA/cm^2, 10 mA/cm^2 and (b) the corresponding specific capacities of the MnO/Co@N-C-based ZAB, respectively.

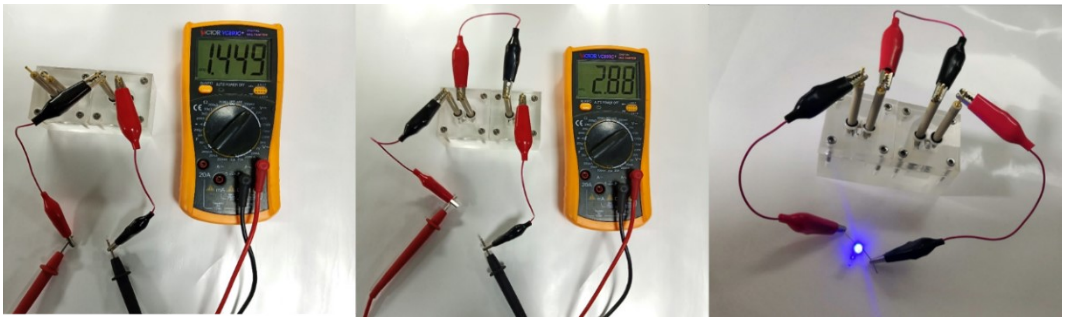

Fig. S14 The photograph of a blue, green and red LED powered by two tandem ZABs.

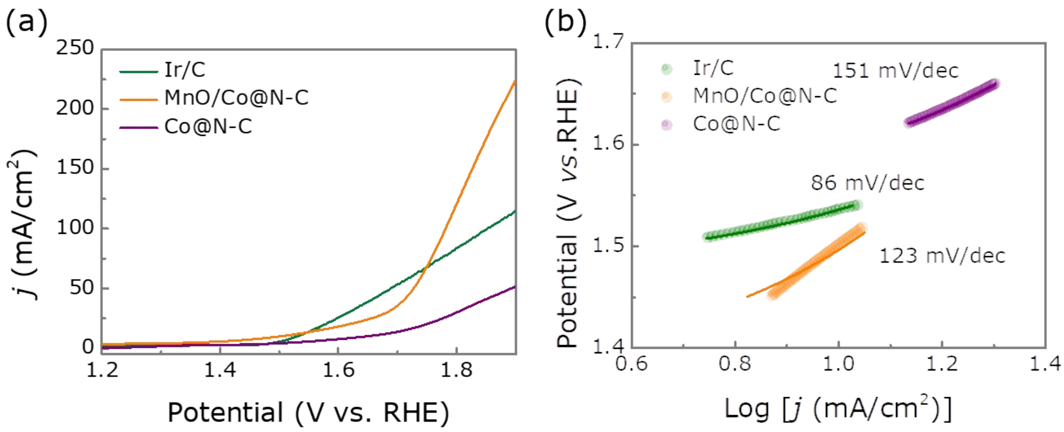

Fig. S15 (a) LSV curves of OER and (b) the corresponding Tafel slopes for MnO/Co@N-C, Co@N-C and Ir/C catalysts.

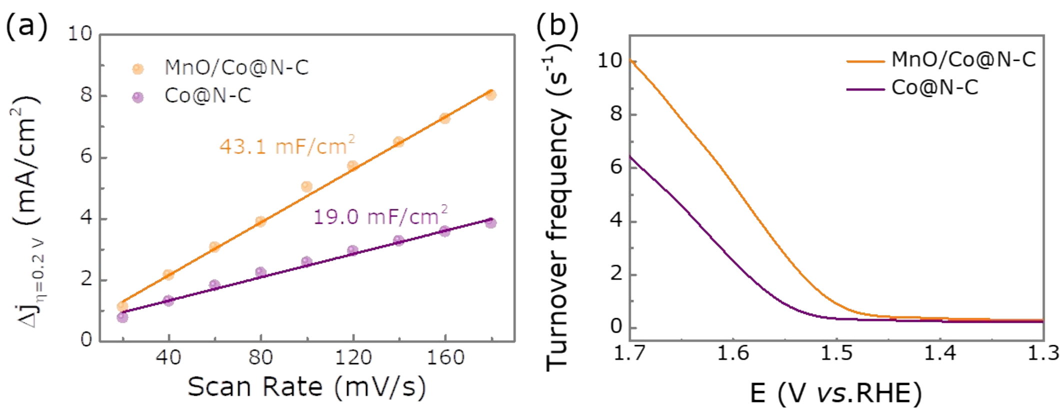

Fig. S16 (a)-(b) ECSA and TOF results of MnO/Co@N-C and Co@N-C catalysts.

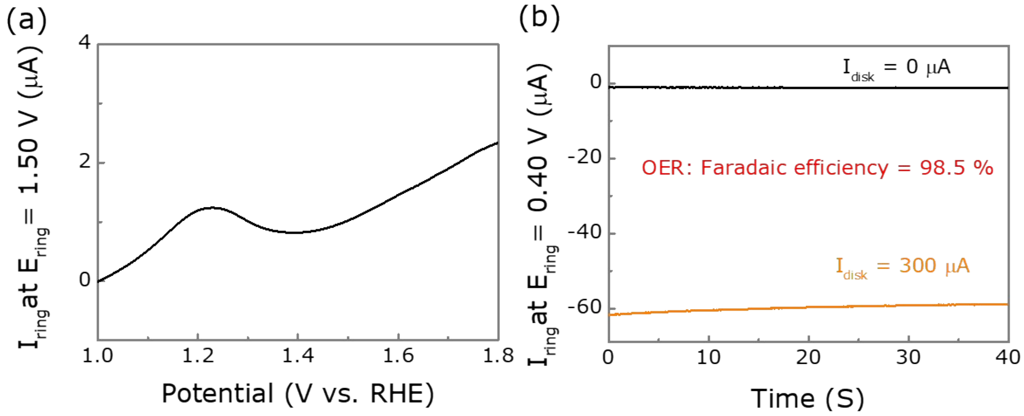

Fig. S17 (a) Ring current of MnO/Co@N-C catalyst on an RRDE (1600 rpm) in O_2-saturated 1 M KOH at a constant potential of 1.50 V *vs.* RHE. (b) Ring current of MnO/Co@N-C catalyst on an RRDE (1600 rpm) in N_2-saturated 1.0 M KOH at a constant potential of 0.4 V *vs.* RHE

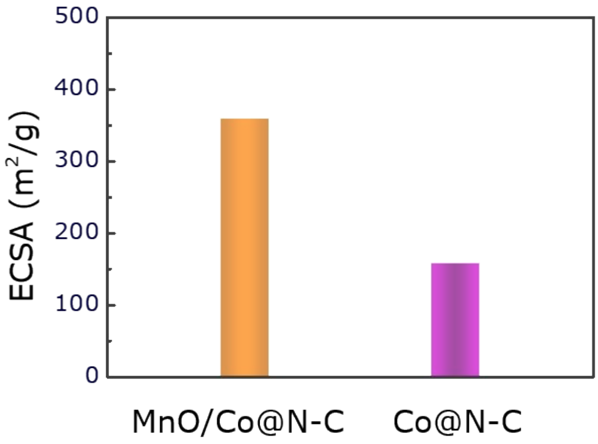

Fig. S18 ECSA results of MnO/Co@N-C and Co@N-C catalysts.

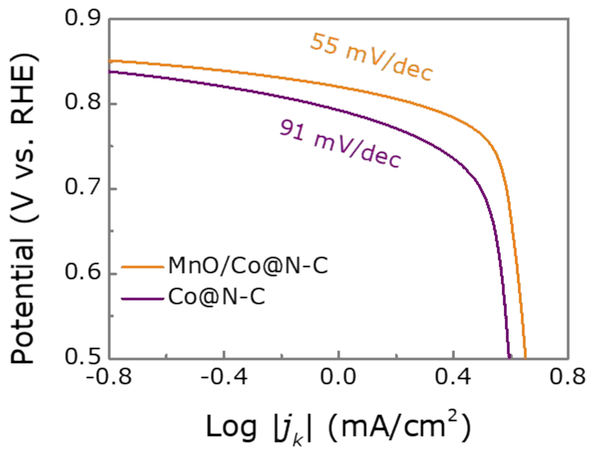

Fig. S19 The Tafel curves of MnO/Co@N-C and Co@N-C catalysts.

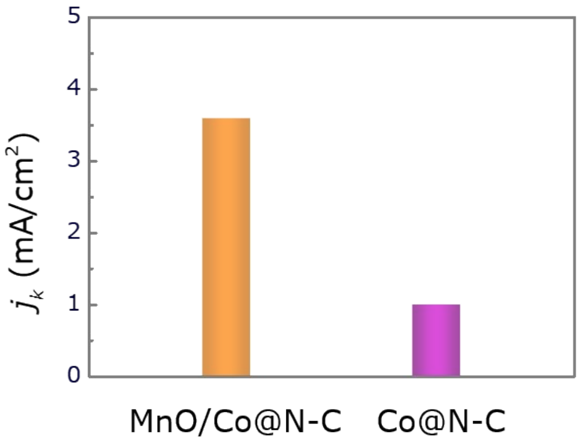

Fig. S20 The Kinetic current density (J_K) of MnO/Co@N-C and Co@N-C catalysts.

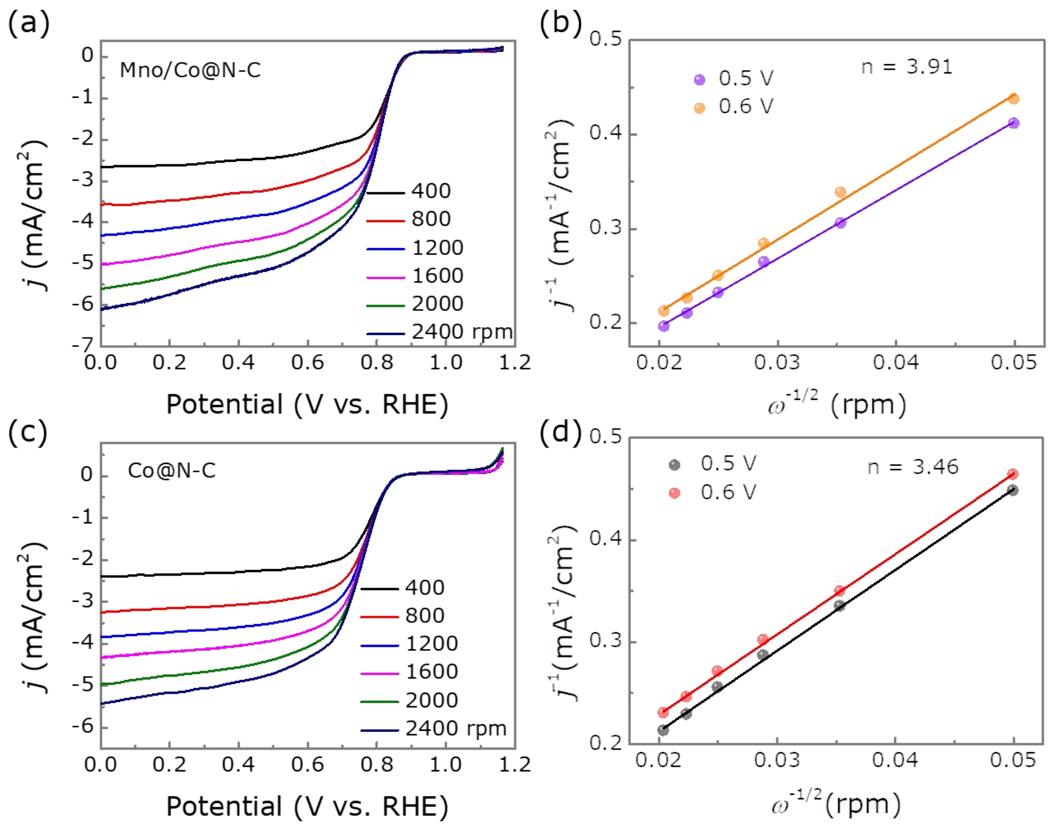

Fig. S21 (a) LSV curves of ORR for MnO/Co@N-C at different rotation speeds and (b) the corresponding Koutecky-Levich plots. (c) LSV curves of ORR for Co@N-C at different rotation speeds and (d) the corresponding Koutecky-Levich plots.

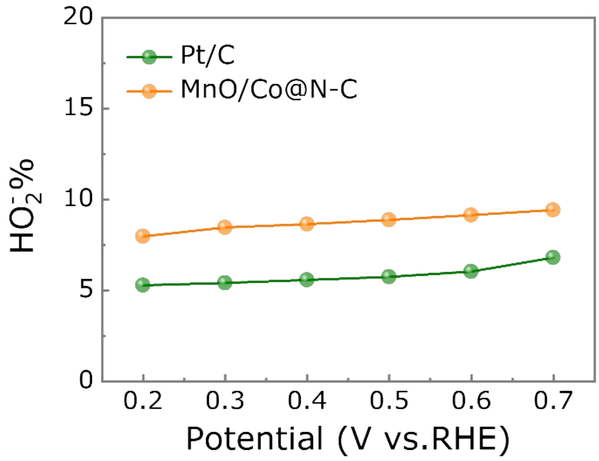

Fig. S22 The yield of HO_2^- for MnO/Co@N-C and Pt/C in O_2 saturated 0.1 M KOH.

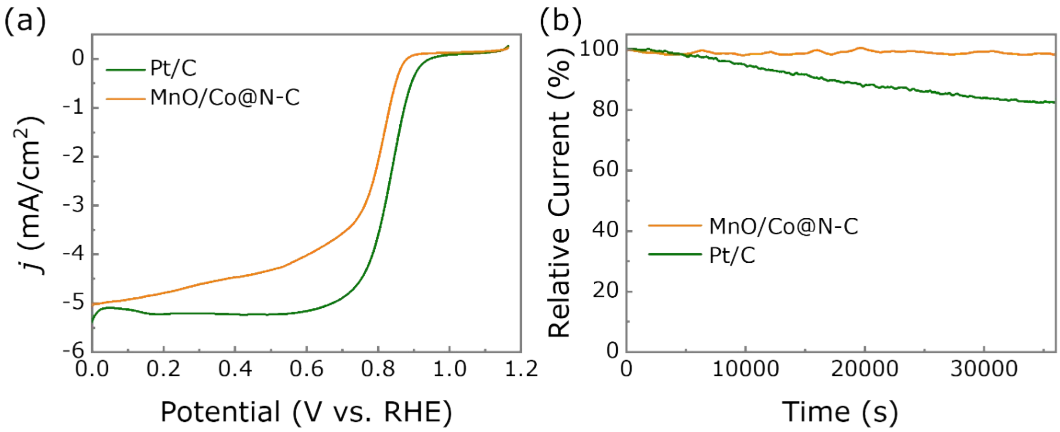

Fig. S23 (a) ORR and (b) i-t curves for the MnO/Co@N-C and Pt/C catalysts.

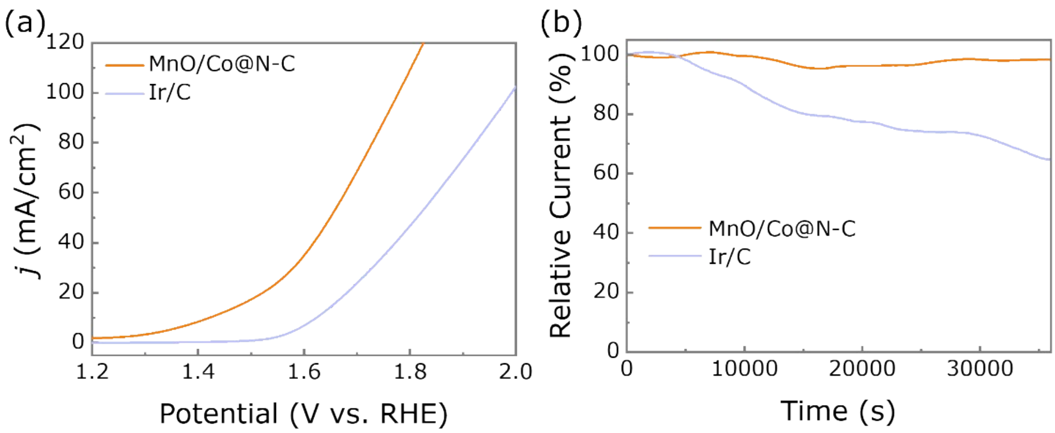

Fig. S24 (a) ORR and (b) i-t curves for the MnO/Co@N-C and Pt/C catalysts.

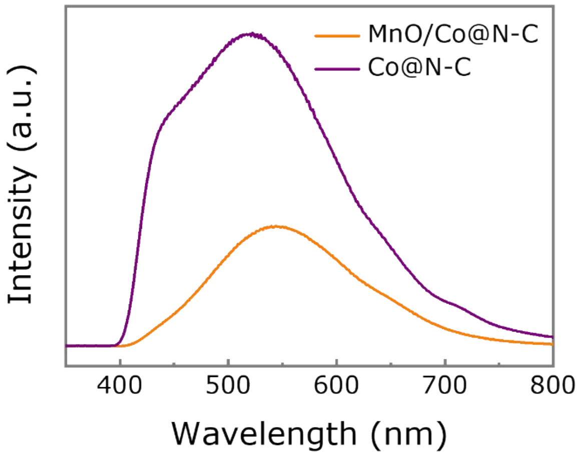

Fig. S25 Photoluminescence spectra of MnO/Co@N-C and Co@N-C catalysts.

Table S1. Comparison of the photo-stimulated ZAB performances of our work and other recently reported catalysts.

Catalysts	Light source	Power density (mW/cm^2)	Cycle performance (at mA/cm^2)	Ref.
MnO/Co@N–C	Metal halide lamp (175 W)	189	1500 cycles (250 h) at 5	The work
CuZIF–67	Xenon lamp (150 W)	~	1000 cycles at 2	1
pTTh/CCB	Xenon lamp (300 W)	27.5	~	2
$TiO_2@In_2Se_3@Ag_3PO$	365 nm (90 mW/cm)	~	210 h at 5	3
4	LED light (LFM375)	~70	200 h at 0.5	4
MoS_2-ONT	Xenon lamp (500 W)	77	100 h at 5	5
FeNi-S,N-HCS		~	600 min at 2	6
$NiCo_2S_4$	AM 1.5 G	~	64 h at 5	7
S-scheme TiO_2-In_2Se_3	LED (50 W)	~28	~64 h at 0.1	8
pTTh				
	AM 1.5 G (100 mW/cm^2)	~	70 h at 20	9
Co_3O_4				
	365 nm (90 mW/cm)	~	22 h at 5	10
PDTB	Xenon lamp (300 W)	~	500 cycles at 0.1	11
$CoMn_2O_4$/Ti-Fe_2O_3				

References

1 R. Ren, G. Liu, J. Kim, R. Ardhi, M. Tran, W. Yang and J. Lee, Photoactive g-C_3N_4/CuZIF-67 Bifunctional Electrocatalyst with Staggered p-n Heterojunction for Rechargeable Zn-Air Batteries, *Appl. Catal. B-Environ.*, 2022, **306**, 121096.

2 S. Hu, J. Shi, R. Yan, S. Pang, Z. Zhang, J. Wang and M. Zhu, Flexible Recharg-eable Photo-Assisted Zinc-Air Batteries Based on Photo-Active pTTh Bifunctional Oxygen Electrocatalyst, *Energy Storage Mater.,* 2024, **65**, 103139.

3 H. Feng, C. Zhang, Z. Liu, J. Sang, S. Xue and P. Chu, A Light-Activated TiO_2@In_2Se_3@Ag_3PO_4 Cathode for High-Performance Zn-Air Batteries, *Chem. Eng. J.,* 2022, **434**, 134650-134660.

4 S. Liang, L. Zheng, L. Song, X. Wang, W. Tu and J. Xu, Accelerated Confined Mass Transfer of MoS_2 1D Nanotube in Photo-Assisted Metal-Air Batteries, *Adv. Mater.,* 2024, **36**, 2307790.

5 S. Zheng, M. Chen, K. Chen, Y. Wu, J. Yu, T. Jiang and M. Wu, Solar-Light-Responsive Zinc-Air Battery with Self-Regulated Charge-Discharge Performance based on Photothermal Effect, *ACS Appl. Mater. Interfaces,* 2023, **15**, 2985-2995.

6 S. Sarawutanukul, C. Tomon, S. Duangdangchote, N. Phattharasupakun and M. Sawangphruk, Rechargeable photoactive Zn-Air batteries using $NiCo_2S_4$ as an efficient bifunctional photocatalyst towards OER/ORR at the cathode, Batteries & Supercaps, 2020, **3**, 541-54.

7 H. Feng, C. Zhang, M. Luo, Y. Hu, Z. Dong, S. Xue and P. Chu, Photo Energy-Enhanced Oxygen Reduction and Evolution Kinetics in Zn-Air Batteries, *ACS Appl. Mater. Interfaces,* 2023, **15**, 6788-6796.

8 D. Zhu, Q. Zhao, G. Fan, S. Zhao, L. Wang and F. Li, Photo-induced oxygen reduction reaction boosts the output voltage of Zn-Air battery, *Angew. Chem. Int. Ed.,* 2019, **131**, 12590-1259.

9 C. Tomon, S. Sarawutanukul, S. Duangdangchote, A. Krittayavathananon and M. Sawangphruk, Photoactive Zn-air batteries using spinel-type cobalt oxide as a bifunctional photocatalyst at the air cathode, *Chem. Commun.* 2019, **55**, 5855-5858.

10 D. Du, S. Zhao, Z. Zhu, F. Li and J. Chen, Photo-Excited Oxygen Reduction and Oxygen Evolution Reactions Enable a High-Performance Zn-Air Battery, *Angew. Chem. Int. Ed.,* 2020, **59**, 18140-18144.

11 X. Wang, P. Li, D. Wang, T. Xie and Y. Lin, $CoMn_2O_4$ Modified Ti-Fe_2O_3 Boosts Charge-Discharge Performance by Enhancing OER in Photo-Assisted Zinc-Air Batteries, *Int. J. Hydrogen Energ.,* 2025, **157**, 150386.